# Solar Spectral Optical Properties of Pigments Part I: Model for Deriving Scattering and Absorption Coefficients from Transmittance and Reflectance Measurements

Ronnen Levinson, Paul Berdahl, and Hashem Akbari
Lawrence Berkeley National Laboratory

June 15, 2004

**Abstract**

The suitability of a pigment for inclusion in "cool" colored coatings with high solar reflectance can be determined from its solar spectral backscattering and absorption coefficients. Pigment characterization is performed by dispersing the pigment into a transparent film, then measuring spectral transmittance and reflectance. Measurements of the reflectance of film samples on black and white substrates are also used. A model for extracting the spectral backscattering coefficient $S$ and absorption coefficient $K$ from spectrometer measurements is presented. Interface reflectances complicate the model. The film's diffuse reflectance and transmittance measurements are used to determine $S$ and $K$ as functions of a wavelength-independent model parameter $\sigma$ that represents the ratio of forward to total scattering. $\sigma$ is used to estimate the rate at which incident collimated light becomes diffuse, and is determined by fitting the measured film reflectance backed by black. A typical value is $\sigma = 0.8$. Then, the measured film reflectance backed by white is compared with a computed value as a self-consistency check. Measurements on several common pigments are used to illustrate the method.

# Nomenclature

## English Symbols

| | |
|---|---|
| $a$ | defined as $(S+K)/S$ |
| $b$ | defined as $(a^2-1)^{\frac{1}{2}}$ |
| $f$ | film |
| $g$ | background |
| $i$ | intensity of total downflux |
| $i_c$ | intensity of collimated downflux (incident direction is downward) |
| $i_d$ | intensity of diffuse downflux |
| $j$ | intensity of total upflux |
| $j_c$ | intensity of collimated upflux |
| $j_d$ | intensity of diffuse upflux |
| $K$ | absorption coefficient |
| $m$ | relative refractive index or wavelength index |
| $M$ | total number of wavelengths |
| $n$ | refractive index |
| $N$ | observed near-infrared reflectance |
| $q$ | fraction of total flux that is diffuse |
| $R$ | reflectance |
| $\tilde{R}_c$ | observed reflectance of collimated light |
| $R_f$ | CRI (continuous refractive index) reflectance of film (absent interface reflectances) |
| $\tilde{R}_f$ | observed reflectance of film |
| $R_{f,\ell}$ | CRI reflectance of film with background $\ell$ |
| $\tilde{R}_{f,\ell}$ | observed reflectance of film with background $\ell$=$b$ (black), $w$ (white), or $v$ (void) |
| $R_g$ | CRI reflectance of background |
| $\tilde{R}_g$ | observed reflectance of background |
| $R_{g,\ell}$ | CRI reflectance of background $\ell$ |
| $\tilde{R}_{g,\ell}$ | observed reflectance of background $\ell$ |
| $R^i$ | reflectance to downflux |
| $R^j$ | reflectance to upflux |
| $R_u$ | CRI reflectance of opaque undercoat |
| $\tilde{R}_u$ | observed reflectance of opaque undercoat |
| $R^\star$ | intermediate value used in computation of reflectance of complex backgrounds |
| $S$ | backscattering coefficient (scattering into opposite hemisphere) |
| $T$ | internal transmittance |
| $\tilde{T}$ | observed transmittance |
| $T^i$ | downflux transmittance |
| $T^j$ | upflux transmittance of upflux |
| $\tilde{T}_c$ | observed collimated flux transmittance |
| $z$ | distance from bottom of film |

### Greek Symbols

| | |
|---|---|
| $\alpha, \beta, \gamma$ | components of multi-layer system |
| $\delta$ | film thickness |
| $\Delta$ | error in intensity gradient or reflectance |
| $\epsilon$ | global error in predicted reflectance |
| $\eta$ | average pathlength parameter |
| $\lambda$ | wavelength (in vacuum) |
| $\mu$ | maximum absolute error in predicted reflectance |
| $\rho$ | density |
| $\sigma$ | forward scattering ratio (fraction of scattered light directed into forward hemisphere) |
| $\tau$ | internal film transmittance |
| $\tau_c$ | internal film collimated transmittance |
| $\chi$ | root-mean-square error in predicted reflectance |
| $\omega$ | reflectance at interface of media with different refractive indices |
| $\omega^i$ | reflectance of interface to downflux |
| $\omega^j$ | reflectance of interface to upflux |
| $\omega_c^i$ | reflectance of interface to collimated downflux |
| $\omega_c^j$ | reflectance of interface to collimated upflux |

# 1 Introduction

Nonwhite pigments with high near-infrared (NIR) reflectance historically have been used to camouflage military surfaces (by mimicking foliage) and to minimize solar heating of dark exterior architectural surfaces, such as colored vinyl siding and gray battleship hulls [1, 2, 3]. In recent years roofing manufacturers have incorporated NIR-reflecting pigments in coatings applied to a variety of nonwhite roofing products, such as metal panels and clay tiles [4, 5, 6, 7, 8, 9]. The work we present here develops and validates a model for computation of solar spectral absorption and backscattering coefficients (current article), which is then applied to wide variety of pigments that may be used in architectural coatings (companion article, Levinson et al. 2004, Solar Spectral Optical Properties of Pigments, Part II: Survey of Common Colorants).

Visible light (400 - 700 nm) accounts for only 43% of the energy in the air-mass 1.5 global solar irradiance spectrum (300 - 2500 nm) typical of North-American insolation [10]; the remainder arrives as near-infrared (700 - 2500 nm, 52%) or ultraviolet (300 - 400 nm, 5%) radiation (Fig. 1). Hence, replacing NIR-absorbing ("conventional") roofing with visually similar, infrared-reflecting ("cool") roofing can significantly reduce building heat gain. A recent study found that increasing the solar reflectance of the roof of a prototypical California nonresidential building from 0.20 (conventional medium gray) to 0.55 (soiled white) yields statewide average annual source energy

savings per unit roof area of 30 MJ/m$^2$; peak power demand savings of 2.1 W/m$^2$; and cost savings (15-year net present value of energy, plus savings achieved by downsizing cooling equipment) of \$6/m$^2$ [11, 12]. A *cool* medium-gray roof with an initial near-infrared reflectance of 0.80 might have a weathered solar reflectance of about 0.42 [11, 13]. Since energy, power, and cost savings are approximately proportional to change in weathered solar reflectance [14], using this cool medium-gray roof (weathered solar reflectance 0.42) in place of a standard medium gray roof (weathered solar reflectance 0.20) would yield about 60% of the white-roof savings, or 18 MJ/m$^2$ source energy, 1.3 W/m$^2$ peak power, and \$3.5/m$^2$ energy and equipment cost. Installing such cool colored roofing on nonresidential new construction in California could yield annual statewide savings of 84 TJ source energy, 5.5 MW peak power, and \$17M energy and equipment cost.

A cool coating must have low visible transmittance to hide its background and low NIR absorptance to minimize NIR heat gain. Cool films may be subclassified as either "NIR-reflecting" or "NIR-transmitting." An NIR-reflecting film is always cool, while an NIR-transmitting film requires an NIR-reflecting background (e.g., a shiny metal or a white coating) to form a colored NIR-reflecting composite [1, 15].

A paint is a dispersion of pigment particles (e.g., titania) in a clear binder, such as acrylic. The propagation of light through pigmented coatings is of natural interest to the coating and colorant industries, and has been extensively studied over the past century. The optical properties of a freely suspended film (i.e., reflectance, transmittance, and absorptance) depend on (a) the real and imaginary refractive indices of the pigment and the binder; (b) the size, shape, and concentration of the pigment particles; and (c) the thickness of the film. These optical properties may be determined either *microscopically* or *macroscopically*.

The microscopic approach applies the principles of electromagnetism to analyze the interaction of light with pigment particles, including interparticle effects (i.e., multiple scattering). Mie theory [16] applies well to spherical pigment particles separated by distances large compared to the light wavelength, but is less useful when particles are closely packed or exhibit either geometric or electromagnetic anisotropy. Knowledge of the detailed scattering cross sections of the pigment particles is useful but not sufficient for the simulation for the reflectance of paint-type coatings, [17, 18]. Most practical colored coatings contain strongly scattering pigments and/or have strongly scattering substrates, making it essential to include multiple scattering effects from the outset.

Furthermore, the pigment particles are often close enough together to make the scattering by neighboring particles electromagnetically interdependent [19].

The macroscopic approach treats the coating as a continuous medium with bulk abilities to absorb and scatter light. One of the simplest and most popular continuum models is the two-flux theory introduced by Schuster in 1905 [20] and popularized by Kubelka and Munk [21, 22, 23, 24, 25]. The Kubelka-Munk (K-M) model describes the one-dimensional, bidirectional propagation of diffuse light through a film by parameterizing the rates at which the film absorbs and/or backscatters light. Details of the angular dependence of the radiative transfer are neglected, as are polarization effects. Only two spectral optical measurements (reflectances over two different backgrounds, or one reflectance and one transmittance) are needed to compute the two parameters (spectral absorption and backscattering per unit length) that predict the spectral reflectance and spectral transmittance of a coating of arbitrary thickness and background. The utility of this model is limited by its assumption that light is diffuse throughout the film, which fails when a weakly-scattering film is illuminated by collimated light from a spectrometer or the sun.

More sophisticated models track both diffuse and collimated fluxes. Three-flux models [26] track two diffuse fluxes and one collimated flux, while four-flux models [27, 28] track two diffuse and two collimated beams. Compared to the K-M model, three- and four-flux theories require additional spectral measurements and spectral parameters, and yield significantly more complex expressions for film reflectance and transmittance. However, they are more accurate than the K-M two-flux model, particularly when applied to films that are both weakly backscattering and weakly absorbing [29].

Color and pigment references [30, 31, 32] and pigment manufacturers [5, 6] typically report the spectral reflectance of a well-hiding (i.e., visibly opaque, or "masstone") coating, and sometimes also that of a tint (mixture with white). This description of the coating's masstone (and tint, if given) is insufficient to determine solar spectral absorption and backscattering coefficients. First, spectral reflectance is typically reported over only the visible spectrum, though manufacturers marketing cool pigments usually report spectral reflectance over the entire solar spectrum. Second, the coating is often NIR-transmitting, making its NIR reflectance dependent on that of its background (typically a primed metal panel). Third, knowledge of a film's opaque reflectance yields only the ratio of its absorption and backscattering coefficients. Determination of both coefficients requires

measurements of either (a) the reflectances of a non-opaque film over two different backgrounds, or (b) the reflectance and transmittance of a non-opaque film.

References sometimes also report the ratio of the absorption and scattering coefficients [22, 33], which is equivalent to reporting opaque reflectance. However, our review of the optics and colorant literature identified only a few published spectra of absorption and backscattering coefficients, such as two for titanium dioxide white [34, 19] and one for quinacridone red [35]. Vendors of propriety color-formulation software [36, 37, 38, 39] have further unpublished K-M coefficient data for the visible spectrum.

A straightforward and useful way to characterize the optical properties of a pigmented coating is to measure its spectral reflectance and transmittance, then calculate its spectral absorptance as 1 - reflectance - transmittance. Pigments with weak or strong NIR absorption can be identified by inspection of the spectral absorptance curve. However, knowledge of the spectral reflectance and transmittance of two differently pigmented films is not sufficient to predict the spectral reflectance and transmittance of a film colored with a mixture of the two pigments. Computation of a mixture optical properties requires the knowledge of the bulk properties of each component pigment (in vehicle), such as the Kubelka-Munk backscattering and absorption coefficients. The simplest such mixture model approximates the backscattering and absorption coefficients of a mixture as the volume-weighted averages of the backscattering and absorption coefficients of its constituents [40].

We balance accuracy and simplicity by introducing a variant of the K-M two-flux model that, while less detailed than true four-flux models, does consider the extent to which incident collimated light has been scattered by passage through the film. This article sets out the theory needed to compute absorption and backscattering coefficients from spectrometer measurements of film reflectance and transmittance, then applies it to several commonly used single-pigment coatings. Model accuracy is checked by comparing the predicted and measured reflectances of each film over various backgrounds. A companion article (Levinson et al. 2004, Solar Spectral Optical Properties of Pigments, Part II: Survey of Common Colorants) considers these characterizations pigment-by-pigment, identifying both cool pigments—i.e., those that can be used to make NIR-reflecting or NIR-transmitting cool coatings—and pigments that should be excluded from cool coatings. Our goal is to provide complete solar spectral absorption and backscattering coefficients describing a large palette of pigments usable for architectural coatings.

## 2 Theory

We present the theory required to compute K-M coefficients from spectrometer measurements in seven stages. Specifically, we

1. review the standard K-M two-flux model and identify the errors that stem from its assumption that light in the film is fully diffuse;
2. summarize the K-M solutions that relate film reflectance and transmittance to absorption and backscattering coefficients;
3. develop the theory needed to adjust the film reflectance and transmittance measured by a spectrometer to correct for "interface" reflectances that occur when light passes to a medium of differing refractive index;
4. show how to calculate the reflectance of a composite background, such as a clear substrate with an opaque undercoat;
5. present a technique for computing the magnitude of interface reflectance of incompletely diffused light, to account for the geometry of light striking the interface;
6. develop a method for estimating the extent to which collimated light is diffused by passage through a scattering film; and
7. summarize our computational algorithm.

The purpose of our measurements and model of radiant transfer in single-pigment coatings is to obtain backscattering and absorption coefficients $S$ and $K$ that approximately characterize the pigment. High precision is not the goal, but a reliable general characterization of each individual pigment is. We cover the solar spectral region from 300 to 2500 nm at 5-nm intervals. Each wavelength is treated independently of all others except for the use of the forward scattering ratio. Since the K-M model applies to diffuse illumination, whereas we are using collimated radiation, the treatment may be expected to be more accurate in strongly scattering films in which a fully diffuse radiation field quickly develops. However, we have used a formulation in which a non-scattering pigment (e.g., a dye) is assigned a $K$ value approximating Beer's law for diffuse radiation traversing

a slab. In summary, we are not expecting precise characterization, but expect to extract consistent, reliable, and practical information for each pigment.

## 2.1 Two-Flux Kubelka-Munk Model Vs. Four-Flux Maheu-Letoulouzan-Gouesbet Model

The one-dimensional propagation of light through a coating is approximated by the two-flux *Kubelka-Munk* (K-M) theory, in which downward and upward beams can be absorbed and/or backscattered as they traverse the film. All light in the film is assumed to be diffuse (subscript $d$), either because the film is diffusely illuminated, or because the film is strongly scattering. The downward diffuse flux $i_d(z)$ and upward diffuse flux $j_d(z)$ within the film are modelled by

$$-\frac{di_d}{dz} = -(K+S)i_d + Sj_d \quad (1)$$

$$\frac{dj_d}{dz} = -(K+S)j_d + Si_d \quad (2)$$

where $K$ and $S$ are coefficients of absorption and backscattering, respectively. The fluxes and coefficients are wavelength-specific.

The *Maheu-Letoulouzan-Gouesbet* (M-L-G) four-flux model [27, 28] removes the K-M assumption that all light in the film is diffuse by tracking two collimated fluxes $(i_c, j_c)$ and two diffuse fluxes $(i_d, j_d)$. Denoting the intensities of the total downwelling flux and total upwelling flux by $i(z) = i_c(z) + i_d(z)$ and $j(z) = j_c(z) + j_d(z)$, respectively, the M-L-G model may be expressed in the form

$$-(\frac{di_c}{dz})_{\mathrm{M-L-G}} = -\eta^{-1}[K + (1-\sigma)^{-1}S]i_c \quad (3)$$

$$(\frac{dj_c}{dz})_{\mathrm{M-L-G}} = -\eta^{-1}[K + (1-\sigma)^{-1}S]j_c \quad (4)$$

$$-(\frac{di}{dz})_{\mathrm{M-L-G}} = -(K+S)(\eta^{-1}i_c + i_d) + S(\eta^{-1}j_c + j_d) \quad (5)$$

$$(\frac{dj}{dz})_{\mathrm{M-L-G}} = -(K+S)(\eta^{-1}j_c + j_d) + S(\eta^{-1}i_c + i_d) \quad (6)$$

The average pathlength parameter $\eta$ is the ratio of the diffuse beam pathlength to the collimated beam pathlength, which equals 2 for perfectly diffuse light [21, 22]. The forward scattering ratio

$\sigma$ is the ratio of light scattered into the forward hemisphere to total scattering. Here, following M-L-G, we have made the simplifying assumption that $\sigma$ is the same for both collimated and diffuse light.

Applying the K-M model to total fluxes $i$ and $j$ (rather than to the purely diffuse fluxes $i_d$ and $j_d$) yields flux gradients

$$-(\frac{di}{dz})_{\mathrm{K-M}} = -(K+S)i + Sj = -(K+S)(i_c+i_d) + S(j_c+j_d) \quad (7)$$

$$(\frac{dj}{dz})_{\mathrm{K-M}} = -(K+S)j + Si = -(K+S)(j_c+j_d) + S(i_c+i_d) \quad (8)$$

with errors

$$\Delta(-\frac{di}{dz}) \equiv (-\frac{di}{dz})_{\mathrm{K-M}} - (-\frac{di}{dz})_{\mathrm{M-L-G}} = -(K+S)(1-\eta^{-1})i_c + S(1-\eta^{-1})j_c \quad (9)$$

$$\Delta(\frac{dj}{dz}) \equiv (\frac{dj}{dz})_{\mathrm{K-M}} - (\frac{dj}{dz})_{\mathrm{M-L-G}} = -(K+S)(1-\eta^{-1})j_c + S(1-\eta^{-1})i_c \quad (10)$$

that arise because the pathlength of collimated light is shorter than that of diffuse light by a factor of $\eta$. Since $1-\eta^{-1} > 0$, applying the K-M model to light that is partially collimated and partially diffuse tends to overestimate both (a) attenuation by absorption and backscattering, and (b) intensification by opposite-beam backscattering.

This study relies mainly on the total-flux K-M model [Eqs. (7) and (8)] because it offers relatively compact solutions for film reflectance and transmittance. However, the M-L-G relations for the collimated fluxes [Eqs. (3) and (4)] are used to estimate the extent to which initially collimated light is diffused by passage through the film.

## 2.2 K-M Model Solutions for Film Reflectance and Transmittance

Consider a film of thickness $\delta$ illuminated from above at $z = \delta$. If illumination comes from a medium of refractive index equal to that of the film, and both $K$ and $S$ are independent of $z$, the reflectance of the film's upper surface to downward illumination is

$$R_f \equiv \left(\frac{j}{i}\right)_{z=\delta} = \frac{1 - R_g(a - b\coth bS\delta)}{a - R_g + b\coth bS\delta} \quad (11)$$

where

$$a \equiv (S+K)/S \tag{12}$$

$$b \equiv (a^2-1)^{\frac{1}{2}} \tag{13}$$

and $R_g \equiv (j_d/i_d)_{z=0}$ is the reflectance of the film's background at $z = 0$. We refer to $R_f$ as the film's "continuous refractive index" (CRI) reflectance, since it assumes that incident light passes to a medium of the same refractive index. The film's *internal transmittance* is

$$\tau \equiv \frac{i_{z=0}}{i_{z=\delta}} = \frac{b}{a\sinh bS\delta + b\cosh bS\delta} \tag{14}$$

## 2.3 Determining Backscattering and Absorption Coefficients from Film Reflectance and Transmittance

A film with CRI reflectance $R_{f,0}$ over a black background ($R_{g,0} = 0$) and CRI reflectance $R_{f,1}$ over a non-black background ($R_{g,1} > 0$) has backscattering and absorption coefficients

$$S = \frac{1}{b\delta}\left(\operatorname{arccoth}\frac{1-aR_{f,0}}{bR_{f,0}}\right) \tag{15}$$

and

$$K = (a-1)S \tag{16}$$

where

$$a = \frac{1}{2}\left[R_{f,1} + \frac{R_{f,0} - R_{f,1} + R_{g,1}}{R_{f,0}R_{g,1}}\right] \tag{17}$$

The value of $R_{f,0}$ (and hence those of $S$ and $K$) may also be obtained from CRI film reflectances $R_{f,1}$ and $R_{f,2}$ over dissimilar, nonzero background reflectances $R_{g,1}$ and $R_{g,2}$:

$$R_{f,0} = \frac{R_{f,1}R_{g,2} - R_{f,2}R_{g,1}}{R_{g,2} + R_{g,1}(R_{f,1}R_{g,2} - R_{f,2}R_{g,2} - 1)} \tag{18}$$

A third approach is to determine $R_{f,0}$ and the K-M coefficients from $R_{f,1}$ and $\tau$:

$$R_{f,0} = \frac{1 + R_{f,1}R_{g,1} - \sqrt{(1-R_{f,1}R_{g,1})^2 + 4(R_{g,1}\tau)^2}}{2R_{g,1}} \tag{19}$$

Using $R_{f,1}$ and $\tau$ to determine $K$ and $S$ can improve accuracy when $R_{f,1} - R_{f,0} \ll 1$ (i.e., $\tau \ll 1$ and/or $R_{g,1} \ll 1$).

The preceding solutions [Eqs. (11)-(19)] may be found in multiple references [21, 22, 23, 24, 25].

If the film is weakly absorbing ($K \to 0$), then $a \to 1$; $b \to 0$; and Eqs. (11), (14) and (15) may be evaluated in the non-absorbing limit:

$$\lim_{K\to 0} R_f = \frac{R_g + (1 - R_g)S\delta}{1 + (1 - R_g)S\delta} \tag{20}$$

$$\lim_{K\to 0} \tau = \frac{1}{1 + S\delta} \tag{21}$$

and

$$\lim_{K\to 0} S = \frac{R_{f,0}}{(1 - R_{f,0})\delta} \tag{22}$$

Similarly, if the film is weakly scattering ($S \to 0$), we obtain

$$\lim_{S\to 0} R_f = \tau^2 R_g = \exp(-2K\delta)R_g \tag{23}$$

$$\lim_{S\to 0} \tau = \exp(-K\delta) \tag{24}$$

and

$$\lim_{S\to 0} K = -\frac{\ln \tau}{\delta} \tag{25}$$

Note that absorption coefficients smaller than $K_{\min} \approx 0.1$ mm$^{-1}$ or greater than $K_{\max} \approx 200$ mm$^{-1}$ are difficult to resolve because reducing $K$ below $K_{\min}$ or increasing $K$ above $K_{\max}$ yields changes in film transmittance and reflectance too small to be accurately measured. For example, Eq. (25) predicts that at these lower and upper absorption-coefficient bounds, a 25-$\mu$m-thick nonscattering film would have internal transmittances of 0.998 and 0.007, respectively. The range of resolvable scattering coefficients has the same lower bound ($S_{\min} \approx 0.1$ mm$^{-1}$) and a significantly higher upper bound ($S_{\max} \approx 4000$ mm$^{-1}$). At these lower and upper scattering-coefficient bounds, Eq. (21) predicts that a 25-$\mu$m-thick nonabsorbing film would have internal transmittances of 0.998 and 0.010, respectively. Thus, computed K-M coefficients will tend to be clipped to within the ranges $K_{\min} \le K \le K_{\max}$ and $S_{\min} \le S \le S_{\max}$.

## 2.4 Correcting Spectrometer Measurements of Film Reflectance and Transmittance for Refractive-Index Discontinuities

Film reflectance measured by an air-filled spectrometer will differ from CRI film reflectance predicted by the K-M model due to the change in refractive index at the air-film interface $z = \delta$. The Saunderson correction [41] relates the film's "observed" reflectance $\tilde{R}_f$—i.e., the value of reflectance that would be observed by an air-filled spectrometer or a pyranometer—to its CRI reflectance $R_f$:

$$\tilde{R}_f = \omega^i + \frac{(1-\omega^i)(1-\omega^j)R_f}{1-\omega^j R_f} \tag{26}$$

$\omega^i$ and $\omega^j$ denote the reflectances of the interface to the downward flux ("downflux") $i(z)$ and upward flux ("upflux") $j(z)$, respectively. Inverting this relationship yields the CRI film reflectance $R_f$ described by the K-M model:

$$R_f = \frac{\omega^i - \tilde{R}_f}{\omega^i + \omega^j(1-\tilde{R}_f) - 1} \tag{27}$$

Computing the internal transmittance $\tau$ from spectrometer measurements is appreciably more complicated. The reflectance $R^i_{1,2}$ and transmittance $T^i_{1,2}$ of downwelling light by a two-layer system $\{1,2\}$ are

$$R^i_{1,2} = R^i_1 + \frac{T^i_1 T^j_1 R^i_2}{1-R^j_1 R^i_2} \tag{28}$$

$$T^i_{1,2} = \frac{T^i_1 T^i_2}{1-R^j_1 R^i_2} \tag{29}$$

where $T^i_1$ and $T^i_2$ are the upper and lower layers' transmittances of downwelling light, $R^i_1$ and $R^i_2$ are their reflectances to downwelling light, and $R^j_1$ is the upper layer's reflectance to upwelling light [22, p.124]. The transmittance of downwelling light by a three-layer system $\{1,2,3\}$ is obtained by applying Eq. (29) first to layer 2 over layer 3, and then to layer 1 over the combined layer $\{2,3\}$:

$$T^i_{1,2,3} = \frac{T^i_1 T^i_{2,3}}{1-R^j_1 R^i_{2,3}} = \frac{T^i_1 T^i_2 T^i_3}{(1-R^j_1 R^i_{2,3})(1-R^j_2 R^i_3)} \tag{30}$$

where the reflectance of the lower system $\{2,3\}$ is given by Eq. (28):

$$R^i_{2,3} = R^i_2 + \frac{T^i_2 T^j_2 R^i_3}{1 - R^j_2 R^i_3} \tag{31}$$

A free-film system (that is, a film surrounded above and below by air) may be considered to have three layers: $\alpha$, the air-film interface at $z = \delta$; $\beta$, the film occupying $0 < z < \delta$; and $\gamma$, the film-air interface at $z = 0$. The film's internal transmittance is non-directional—i.e.,

$$\tau = T_\beta = T^i_\beta = T^j_\beta \tag{32}$$

If the film has uniform absorption and backscattering coefficients (i.e., $dK/dz = dS/dz = 0$), its reflectance is also non-directional [22, pp.123-127]:

$$R_\beta = R^i_\beta = R^j_\beta \tag{33}$$

It can be shown by comparing the bilayer film reflectances $R_f$ and $R^i_{\alpha,\beta}$ predicted by Eqs. (11) and (28) that

$$R_\beta = R_{f,0} \tag{34}$$

Since the interfaces are non-absorbing,

$$T^i_\alpha = 1 - R^i_\alpha \tag{35}$$

$$T^i_\gamma = 1 - R^i_\gamma \tag{36}$$

Eqs. (30)-(36) can be solved to obtain the film's internal transmittance $\tau$ from the film's *observed transmittance* $\tilde{T} = T^i_{\alpha,\beta,\gamma}$, yielding

$$\tau = \frac{-(1 - R^i_\alpha)(1 - R^i_\gamma) + \sqrt{\left[(1 - R^i_\alpha)(1 - R^i_\gamma)\right]^2 + 4R^j_\alpha R^i_\gamma (1 - R_{f,0} R^i_\gamma)(1 - R^j_\alpha R_{f,0})\tilde{T}^2}}{2R^j_\alpha R^i_\gamma \tilde{T}} \tag{37}$$

where $R^i_\alpha = \omega^i_\delta$, $R^j_\alpha = \omega^j_\delta$, and $R^i_\gamma = \omega^i_0$.

A film that lies on a clear substrate with air above the film and below the substrate is equivalent

to a free-film system in which the film-substrate interface, $\gamma_a$, and the substrate-air interface, $\gamma_b$, comprise the third layer $\gamma$. We obtain $\tau$ by evaluating Eq. (37) with $R^i_\gamma$ given by Eq. (28):

$$R^i_\gamma = R^i_{\gamma_a,\gamma_b} = R^i_{\gamma_a} + \frac{T^i_{\gamma_a} T^j_{\gamma_a} R^i_{\gamma_b}}{1 - R^j_{\gamma_a} R^i_{\gamma_b}} = R^i_{\gamma_a} + \frac{(1 - R^i_{\gamma_a})(1 - R^j_{\gamma_a}) R^i_{\gamma_b}}{1 - R^j_{\gamma_a} R^i_{\gamma_b}} \tag{38}$$

where $R^i_{\gamma_a} = \omega_{\text{film}\to\text{substrate}}$, $R^j_{\gamma_a} = \omega_{\text{substrate}\to\text{film}}$, and $R^i_{\gamma_b} = \omega_{\text{substrate}\to\text{air}}$.

Eq. (19) expresses film reflectance over black, $R_{f,0}$, in terms of internal transmittance $\tau$, while Eq. (37) expresses $\tau$ in terms of $R_{f,0}$. Simultaneous solution yields

$$R_{f,0} = \frac{A - B\sqrt{C}}{D} \tag{39}$$

where

$$\begin{aligned}
A &= \left(1 - R^i_\alpha\right)^2 \left(1 - R^i_\gamma\right)^2 \left(1 + R_{f,1} R_{g,1}\right) R_{g,1} \\
&\quad + 2 \left(R_{g,1} - R^j_\alpha R^i_\gamma R_{f,1}\right) \left(\left[\left(1 + R_{f,1} R_{g,1}\right) R^i_\gamma - R_{g,1}\right] R^j_\alpha - R^i_\gamma R_{g,1}\right) \tilde{T}^2 \\
B &= \left(1 - R^i_\alpha\right) \left(1 - R^i_\gamma\right) R_{g,1} \\
C &= \left(1 - R^i_\alpha\right)^2 \left(1 - R^i_\gamma\right)^2 \left(1 + R_{f,1} R_{g,1}\right)^2 \\
&\quad + 4 \left(1 - R^j_\alpha R_{f,1}\right) \left(1 - R^i_\gamma R_{f,1}\right) \left(R^j_\alpha - R_{g,1}\right) \left(R^i_\gamma - R_{g,1}\right) \tilde{T}^2 \\
D &= 2 \left[\left(1 - R^i_\alpha\right)^2 \left(1 - R^i_\gamma\right)^2 R^2_{g,1} - \left(R^i_\gamma R_{g,1} - R^j_\alpha \left[\left(1 + R_{f,1} R_{g,1}\right) R^i_\gamma - R_{g,1}\right]\right) \tilde{T}^2\right]
\end{aligned}$$

The internal transmittance is obtained by substituting the result of Eq. (39) into Eq. (37).

## 2.5 Computing Background Reflectance

The film's background reflectance $R_g$ naturally depends on what lies below the film. There are four configurations relevant to this study, depending on the presence or absence of (a) a transparent substrate below the film and (b) an opaque undercoat below the film or film-substrate system.

1. **No substrate or undercoat**. $R_g$ equals the reflectance of the film-air interface at the film bottom $z = 0$:

$$R_g = \omega_{\text{film}\to\text{air}} \tag{40}$$

2. **Undercoat only**. $R_g$ equals the undercoat's CRI reflectance

$$R_u = \frac{\omega^i - \tilde{R}_u}{\omega^i + \omega^j(1 - \tilde{R}_u) - 1} \tag{41}$$

where $\omega^i = \omega_{\text{air}\to\text{undercoat}}$, $\omega^j = \omega_{\text{undercoat}\to\text{air}}$, and $\tilde{R}_u$ is the undercoat's observed reflectance.

3. **Substrate with undercoat**. We compute $R_g$ in two stages. First, we apply the Saunderson correction [Eq. (26)] to $R_u$ to account for the substrate-undercoat interface:

$$R^\star = \omega^i + \frac{(1-\omega^i)(1-\omega^j)R_u}{1-\omega^j R_u} \tag{42}$$

where $\omega^i = \omega_{\text{substrate}\to\text{undercoat}}$ and $\omega^j = \omega_{\text{undercoat}\to\text{substrate}}$. Next, we apply the Saunderson correction to $R^\star$ to account for the film-substrate interface:

$$R_g = \omega^i + \frac{(1-\omega^i)(1-\omega^j)R^\star}{1-\omega^j R^\star} \tag{43}$$

where $\omega^i = \omega_{\text{film}\to\text{substrate}}$ and $\omega^j = \omega_{\text{substrate}\to\text{film}}$.

4. **Substrate only**. Replacing the undercoat in the previous configuration with a substrate-air interface,

$$R^\star = \omega_{\text{substrate}\to\text{air}} \tag{44}$$

We then evaluate Eq. (43) as before to obtain $R_g$.

## 2.6 Estimating Interface Reflectance Resulting from Change in Refractive Index

Light striking a smooth boundary separating a medium of refractive index $n_0$ from a medium of another refractive index $n_1$ will be partly reflected. The magnitude of this "interface reflectance" $\omega$ depends on $n_0$, $n_1$, and the angular distribution of the light. If the light is perfectly *collimated* (indicated by subscript $c$), the normal interface reflectance will be

$$\omega_{c,n_0\to n_1} = \left(\frac{n_1 - n_0}{n_1 + n_0}\right)^2 \tag{45}$$

If the light is perfectly *diffuse* (subscript $d$), the reflectance depends on whether the light is passing from low index to high index ($n_0 < n_1$), or vice-versa ($n_0 > n_1$). Let

$$\begin{aligned} f(m) &= \frac{1}{2} + \frac{(m-1)(3m+1)}{6(m+1)^2} + \left[\frac{m^2(m^2-1)^2}{(m^2+1)^3}\right]\log\frac{m-1}{m+1} \\ &\quad - \frac{2m^3(m^2+2m-1)}{(m^2+1)(m^4-1)} + \left[\frac{8m^4(m^4+1)}{(m^2+1)(m^4-1)^2}\right]\log m \end{aligned} \tag{46}$$

Then [26][22, pp.11-15]

$$\omega_{d,n_0\to n_1} = \begin{cases} f(n_1/n_0) & n_0 < n_1 \\ \\ 1-(n_1/n_0)^2\left[1-f(n_0/n_1)\right] & n_0 > n_1 \end{cases} \tag{47}$$

An initially collimated beam (say, that generated by a spectrometer) that has passed through a scattering medium will be partially diffuse. We propose approximating the interface reflectance to light with diffuse fraction $q$ by

$$\omega_{n_0\to n_1}(q) = (1-q)\times\omega_{c,n_0\to n_1} + q\times\omega_{d,n_0\to n_1} \tag{48}$$

Perfectly collimated light has $q = 0$, while perfectly diffuse light has $q = 1$.

Light downwelling through a film system passes from air ($n = 1$) to a paint resin (e.g., acrylic or polyvinylidene fluoride [PVDF], $n = 1.5$); to a transparent substrate, if present (e.g., polyester, $n = 1.65$); and to either an opaque paint undercoat ($n = 1.5$) or a void—i.e., an air-filled black body cavity ($n = 1$). Upwelling light undergoes an analogous series of interface reflections. Interface reflectances are minor when light is perfectly collimated (e.g., $\omega_{c,\text{air}\leftrightarrow\text{resin}} = 0.04$) and when light is perfectly diffuse but passes to a medium of higher $n$ (e.g., $\omega_{d,\text{air}\to\text{resin}} = 0.09$). However, total internal reflectance of rays that strike the interface at supercritical angles ($\theta > \arcsin[n_0/n_1]$) yields large reflectances when diffuse light passes to a medium of lower $n$ (Table 1). For example, $\omega_{d,\text{resin}\to\text{air}}$ has a theoretical value of about 0.60 when light is perfectly diffuse. It should be noted that there is significant uncertainty in the true magnitude of this partial total internal reflectance. For example, studies of light diffused by opal glasses ($n = 1.5$) have measured glass-air interface reflectances ranging from 0.3 to 0.6 [42, 43].

Table 1: *Reflection due to change in refractive index at a smooth interface.*

| **Collimated Light** ($q = 0$) | *To* | | |
|---|---|---|---|
| *From* | $n = 1$ (air) | $n = 1.5$ (paint resin) | $n = 1.65$ (polyester substrate) |
| $n = 1$ (air) | 0 | 0.04 | 0.06 |
| $n = 1.5$ (paint resin) | 0.04 | 0 | 0.002 |
| $n = 1.65$ (polyester substrate) | 0.06 | 0.002 | 0 |
| **Diffuse Light** ($q = 1$) | *To* | | |
| *From* | $n = 1$ (air) | $n = 1.5$ (paint resin) | $n = 1.65$ (polyester substrate) |
| $n = 1$ (air) | 0 | 0.09 | 0.11 |
| $n = 1.5$ (paint resin) | 0.60 | 0 | 0.03 |
| $n = 1.65$ (polyester substrate) | 0.67 | 0.19 | 0 |

Since a spectrometer illuminates a film with collimated light, the diffuse fraction of downwelling striking the air–film interface at ($z = \delta$) is $q_\delta^i = 0$. The diffuse fractions at the other interfaces depend on the nature of the film and its background. For example, consider the following three cases for a film system *without substrate*.

1. **Non-scattering film without undercoat**. If $S = 0$ and the film has no undercoat, the downflux and upflux will be fully collimated at all interfaces.

2. **Scattering film without undercoat**. If $S > 0$, the downwelling light striking the film–air interface at the bottom of the film will be partly diffuse. Since this interface ($n = 1.5$ to $n = 1$) preferentially reflects diffuse light, the upwelling light striking the film–air interface at the top of the film will be almost perfectly diffuse unless the scattering is very weak.

3. **Scattering or non-scattering film with undercoat**. If the film has an opaque, diffusely reflecting undercoat (e.g., black or white paint), upwelling light striking the film–air interface at the top of the film will be perfectly diffuse. There is no refractive-index change at the bottom of the film, and hence no interface reflection to consider.

The above description applies also to a film that has a substrate (e.g., glass) with refractive index equal to that of the film. A similar but somewhat more complex accounting is required when the film has a substrate (e.g., polyester) with refractive index different from that of the film.

The diffuse fraction of light striking the various refractive-index interfaces of a film that does not have an undercoat can be estimated by comparing the intensities of the collimated and total fluxes at these interfaces. The diffuse fraction of downwelling light striking the film–air or film–(substrate

+ air) interface at the bottom of the film is

$$q_0^i = 1 - i_c(0)/i(0) \tag{49}$$

and that of upwelling light striking the film–air interface at the top of the film is

$$q_\delta^j = 1 - j_c(\delta)/j(\delta) \tag{50}$$

Since the film's observed transmittance—i.e., the ratio of flux leaving the bottom of the film to the *unit* flux incident on the top of the film—is $\tilde{T} = (1 - \omega_0^i)i(0)$ and observed reflectance is $\tilde{R}_f = \omega_\delta^i + (1 - \omega_\delta^j)j(\delta)$, the total downflux at the bottom of the film and upflux at the top of the film may be expressed in terms of the film measurements as

$$i(0) = \tilde{T}/(1 - \omega_0^i) \tag{51}$$

and

$$j(\delta) = (\tilde{R}_f - \omega_\delta^i)/(1 - \omega_\delta^j) \tag{52}$$

We take the following approach to determine $i_c(0)$ and $j_c(\delta)$—i.e., the collimated downflux just inside the bottom of the film, and the collimated upflux just inside the top of the film. In the K-M and M-L-G models, the film's CRI reflectance of collimated light is zero, because backscattering is assumed to convert collimated light into oppositely directed diffuse light. The film's *observed* reflectance and transmittance of collimated light, $\tilde{R}_c$ and $\tilde{T}_c$, can be determined by applying Eqs. (28) and (29) to the system's three layers—air-film interface, film, and film-air or film-(substrate+air) interface. This yields

$$i_c(0) = \tilde{T}_c/(1 - \omega_{c,0}^i) = \frac{(1 - \omega_{c,\delta}^i)\tau_c}{1 - \tau_c^2 \omega_{c,\delta}^j \omega_{c,0}^i} \tag{53}$$

and

$$j_c(\delta) = (\tilde{R}_c - \omega_{c,\delta}^i)/(1 - \omega_{c,\delta}^j) = \frac{(1 - \omega_{c,\delta}^i)\omega_{c,0}^i \tau_c^2}{1 - \tau_c^2 \omega_{c,\delta}^j \omega_{c,0}^i} \tag{54}$$

We estimate the internal transmittance of collimated light, $\tau_c$, from Eq. (3), yielding

$$\tau_c = \exp\left\{-[K + (1-\sigma)^{-1}S]\delta/\eta\right\} \tag{55}$$

where the average pathlength parameter $\eta$ is assumed to be 2. The forward scattering ratio $\sigma$ is a fitted parameter, as described in the next section.

## 2.7 Algorithms

Spectral K-M coefficients can be computed from either (A) observed spectral reflectance and transmittance over a void background; or (B) observed spectral reflectances over two different backgrounds (e.g., opaque black and opaque white). In Method A, we must determine the internal transmittance and CRI reflectance of a film with a void background, which in turn requires estimation of forward scattering ratio $\sigma$, spectral diffuse fractions, and spectral interface reflectances. This is much more complex than Method B, in which we need only calculate CRI film reflectances with the assumption that light exiting the film-air interface is fully diffuse. However, there are several advantages to Method A. First, the two optical measurements are made on the same specimen, which ensures that the film properties used to compute the K-M coefficients are based on samples of the same thickness. Second, measuring both reflectance and transmittance yields absorptance, which directly indicates whether a film is hot or cool. Third, since light reflected from a film's background makes two passes through the film, it is more accurate to characterize a film with one reflectance and one transmittance than with two reflectances. This is important when the film is nearly opaque, and/or the two backgrounds have similar reflectance (e.g., in the UV, where a white background is poorly reflecting). Hence, we use Method A.

Taking as inputs the observed spectral reflectance and transmittance of a film with a void background, we seek (a) spectral values of the K-M coefficients, $K(\lambda)$ and $S(\lambda)$; and (b) a wavelength-independent value of $\sigma$ that minimizes the global error in the predicted value of a third observed spectral film reflectance, such as that over a black background. Algorithm I describes the process for seeking the spectral coefficients given $\sigma$; algorithm II, which calls algorithm I, describes the optimization of $\sigma$.

**I. Determining Spectral K-M Coefficients Given a Non-Spectral Forward Scattering**

**Ratio**. We perform the following at each wavelength of interest. If the film is opaque, we report only its CRI reflectance, since in this case it is not possible to calculate both $K$ and $S$. Otherwise, we compute initial values of interface reflectances by assuming that the light is everywhere collimated. Let subscripts $v$, $b$, and $w$ refer to void, opaque black, and opaque white backgrounds, respectively. We iterate the following six steps until either (a) the fractional changes in $K$ and $S$ fall below some threshold (e.g., 1%), or (b) reaching an iteration limit (say, 5).

1. Use the inverse Saunderson correction [Eq. (27)] to calculate CRI film reflectances $R_{f,v}$ and $R_{f,b}$ from their corresponding observed values.
2. Calculate background reflectances $R_{g,v}$ and $R_{g,b}$ from Eqs. (40)-(44).
3. Calculate $R_{f,0}$ and $\tau$ from Eqs. (39) and (37), respectively.
4. If $R_{f,0} > 0$:
   (a) Calculate $a$ from Eq. (17).
   (b) If $a > 1$, calculate $b$, $S$, and $K$ from Eqs. (13), (15), and (16), respectively.
   (c) If $a \leq 1$, assume that $K = 0$ and evaluate $S$ from Eq. (22).
5. If $R_{f,0} \leq 0$, assume that $S = 0$ and evaluate $\tau$ and $K$ from Eqs. (24) and (25), respectively.
6. Calculate new values of the interface reflectances $\omega_\delta^j$ and $\omega_0^i$ by applying Eqs. (49)-(55) to the current values of $S$, $K$, $\omega_\delta^j$ and $\omega_0^i$.

When the iterations finish, we calculate the CRI film reflectance over each background (void, black, and white) from $K$ and/or $S$ using Eq. (11), (20), or (23). We then calculate the corresponding observed reflectances via the Saunderson correction [Eq. (26)].

**II. Determining Non-Spectral Forward Scattering Ratio**. We choose the value of $\sigma$ between 0 and 1 that minimizes the difference between the measured and calculated observed values of the film's reflectance over black. We seek a wavelength-independent value of $\sigma$ to keep the model simple. Specifically, we minimize the global error $\epsilon = \chi + \mu$ over $M$ wavelengths, where

$$\chi = \left( \frac{1}{M} \sum_{m=1}^{M} \Delta_m^2 \right)^{\frac{1}{2}} \tag{56}$$

$$\mu = \max|\Delta_m|, m = 1 \ldots M \tag{57}$$

and

$$\Delta_m = \tilde{R}_{f,\mathrm{calc}}(\lambda_m) - \tilde{R}_{f,\mathrm{meas}}(\lambda_m) \tag{58}$$

Our choice of global error norm $\epsilon$ helps avoid values of $\sigma$ that yield a small RMS error $\chi$ but generate large $\Delta_m$ at one or more wavelengths.

# 3 Experiment

The optical properties of 87 pigment films—4 white, 21 black or brown, 14 blue or purple, 11 green, 9 red or orange, 14 yellow, and 14 pearlescent—were characterized by computing spectral K-M coefficients and non-spectral forward scattering ratios from spectral measurements of film reflectance and transmittance.

## 3.1 Sample Preparation

Twenty-six polyvinylidene fluoride (PVDF) resin paint films were provided by a manufacturer of coil-coating paints. Another 34 acrylic paints were purchased as artist colors, and the remaining 27 coatings were acrylic-base letdowns (dilutions) of cool (primarily metal-oxide) pigment dispersions from pigment manufacturers. The PVDF and acrylic resins in these coatings each have refractive index $n = 1.5$.

Each PVDF film was prepared by (a) using a wirewound rod (a long cylindrical rod covered with a single winding of tightly wrapped wire) to coat an aluminum substrate; (b) baking and quenching the coating; (c) dissolving the aluminum with hydrochloric acid; and then (d) rinsing the film with water. We prepared a substrated film of each acrylic paint by coating a 25-$\mu$m thick sheet of clear Mylar-D® polyester ($n = 1.65$; nonscattering; absorptance $< 0.02$ @ 400-2,100 nm, $< 0.07$ @ 325-400 nm and 2,100-2,500 nm; strongly absorbing below 325 nm, approaching 0.9 absorptance at 300 nm) with a wirewound rod, then allowing the paint to dry overnight at room temperature. Film thicknesses (excluding substrate, if any) ranged from 10 to 37 $\mu$m.

Three 35-mm × 40-mm samples of each film were placed in glassless slide mounts, and the central thickness of each sample measured with a micrometer (accuracy ± 2 $\mu$m). The back of the first sample was coated with an opaque layer of black paint (synthetic black iron oxide, 0.9 ± 0.2 mm, non-reflecting); the back of the second sample was coated with an opaque layer of white

paint (titanium dioxide, 1.6 ± 0.4 mm; spectral reflectance shown in Fig. 2); and the back of the third sample was not coated. These film backgrounds are denoted "black," "white," and "void," respectively. The final term refers to the state of having no undercoating, in which case light passing through the film enters a light trap when the film's reflectance is measured in a spectrometer.

### 3.2 Optical Measurements and Corrections

A Perkin-Elmer Lambda-900 UV-VIS-NIR spectrometer equipped with a 150-mm Labsphere integrating sphere was used to measure each film's reflectance over black, reflectance over white, reflectance over void, and transmittance. The specular components of both reflectance and transmittance were included. Optical measurements were performed at 5-nm intervals over the solar spectrum (300 - 2,500 nm), and were subject to two corrections.

**A. Removing Thin-Film Interference**. First, thin-film interference induced by the uniform thickness of the polyester substrate creates noticeable ripples in the measured reflectance and transmittance of acrylic paints at wavelengths where the film is highly transmitting. Hence, the measured spectral reflectance and transmittance of films with substrates were smoothed by convolution with a discrete Gaussian filter when the measured spectral transmittance exceeded a threshold. The filter width (± 10 wavelengths), spread (half width/3), and transmittance threshold (0.7) were sized to remove as much of the thin-film interference as possible while minimizing distortion of true spectral features.

**B. Removing Detector-Transition Discontinuities**. The spectrometer has two adjacent light detectors at the bottom of its integrating sphere: a UV-VIS photomultiplier tube for wavelengths below 860 nm, and a lead sulfide NIR sensor for wavelengths of 860 nm and greater. It is common to observe a blip (i.e., a small but spectrally rapid change) in measured reflectance and/or transmittance near this detector transition. Since some films with blips also exhibited several slightly negative values of absorptance (1 - reflectance - transmittance) in the NIR, we concluded that the NIR detector's signal was more likely in error.

We suspect that this discontinuity stems from the design of the integrating sphere. First, the baffle that shields the UV-VIS sensor from beam radiation may imperfectly shield the neighboring NIR sensor. Second, the efficiency of integrating sphere varies with the exact location of the reflected specular spot, which in turn depends on target texture and curvature [44]. Errors are

roughly ±1% of the reflected specular component in most of the solar spectrum, and closer to ±2% beyond 2,000 nm where the reflectance of the sphere's Spectralon® surface is a little lower. (These estimates are based on the reflectance of a mirror that is tipped slightly to move the specular spot by several millimeters.) Since the phototube detector used for the UV and visible measurements and the PbSe detector covering the infrared beyond 860 nm are not in exactly the same position within the integrating sphere, the integrating sphere efficiency errors can be different, resulting in small discontinuities near 860 nm.

We adjusted the reflectances and transmittances measured by the NIR detector by first extrapolating a "corrected" value at 860 nm from the values at 850 and 855 nm, then adding the difference between the corrected and measured 860-nm values to measured values at all wavelengths greater than 860 nm. This correction eliminated the slightly negative absorptances.

Observations of negative absorbance may also result if the spot at which the film transmittance is measured is thinner than the spot at which film reflectance is measured. Consider a non-absorbing sample with exactly 0.5 transmittance and 0.5 reflectance. If the transmittance measurement is made on a part of the sample that is 5% thinner than the spot at which reflectance is measured, the transmittance measurement may be too large by about 0.025, and apparent sample absorptance (1-reflectance-transmittance) may appear to be negative.

### 3.3 Computing Pigment Volume Concentration

The pigment volume concentration (PVC) of each dry coating was computed either from the specific gravities of paint, pigment, and binder, or from pigment-load information supplied by the manufacturer.

## 4 Results

Model performance was gauged by examining (a) spectral characterizations of six representative pigments and (b) the accuracy with which computed K-M coefficients predict film reflectance over black and white backgrounds. The six sample results are presented below. Spectral characterizations of all 87 pigmented films are reported in a companion article (Levinson et al. 2004, Solar Spectral Optical Properties of Pigments, Part II: Survey of Common Colorants).

### 4.1 Detailed Spectral Analyses of Six Representative Pigments

The measured and computed spectral properties of films colored with each of six pigments—(a) titanium dioxide white, (b) carbon black, (c) iron oxide red, (d) phthalo blue, (e) phthalo green, and (f) mica flakes coated with titanium dioxide—are shown in Fig. 3. Charted for each coating are (I) measured optical properties of a film over void; (II) computed K-M coefficients; (III) computed diffuse fractions and interface reflectances; and (IV) measured and computed values of reflectance over black and white backgrounds.

*Chart I* shows the film's measured reflectance $\tilde{R}_{f,v}(\lambda)$ and measured transmittance $\tilde{T}(\lambda)$ over void, which are used to compute K-M coefficients, and computed absorptance, $\tilde{A}(\lambda) = 1 - \tilde{R}_{f,v}(\lambda) - \tilde{T}(\lambda)$. Its legend tabulates solar ("s"), UV ("u"), visible ("v"), and NIR ("n") spectrally integrated values computed by weighting each property with the air-mass 1.5 solar spectral irradiance shown in Fig. 1.

*Chart II* presents backscattering and absorption coefficients $S(\lambda)$ and $K(\lambda)$, along with the non-spectral forward scattering ratio $\sigma$ that minimizes the error in predicted reflectance over black. In this graph, non-zero K-M coefficients are assigned a minimum value of 0.1 $\text{mm}^{-1}$, which is an estimate of the smallest resolvable non-zero value for $K$ and $S$ (cf. §2.3). At wavelengths where only $S$ is shown, $K$ was assumed to be zero, and vice versa. Where the film is opaque, neither $S$ nor $K$ is shown.

*Chart III* shows a few of the ancillary properties computed in the process of generating K-M coefficients, namely the diffuse fraction $q$ and the interface reflectance $\omega$ for fluxes exiting the top and bottom of the void-backed film. These interface reflectances are used to correct the measured values of film reflectance and transmittance during computation of $K$ and $S$ (cf. §2.4).

*Chart IV* compares values of over-black and over-white observed reflectances $\tilde{R}_{f,b}(\lambda)$ and $\tilde{R}_{f,w}(\lambda)$ computed from the K-M coefficients to values measured with the spectrometer. The computed reflectance over black (ROB) is fitted to its corresponding measured value by the choice of the non-spectral forward scattering ratio. However, the computed reflectance over white (ROW) is independent of the measured ROW, since the latter property is not used to calculate K-M coefficients. Hence, the error in ROW serves as a strong check for the accuracy of $K$ and $S$, while the error in ROB serves as a weaker check. Also shown in this chart are the RMS errors $\chi_w$ and $\chi_b$ in

predictions of ROW and ROB, and the measured over-white and over-black NIR reflectances $N_w$ and $N_b$.

**A. Titanium Dioxide White.** Titanium dioxide white (Fig. 3a) scatters strongly in most of the solar spectrum but absorbs strongly in the UV (below 400 nm). In most of the visible and infrared spectra there is little absorption. The inferred scattering coefficient $S$ declines by two orders of magnitude between 400 and 2500 nm, which is typical behavior for scattering pigments. For generic $TiO_2$ (rutile) we have 200-nm particles of refractive index $\approx 2.7$. For well-dispersed particles that are much smaller than the wavelength, we expect Rayleigh behavior in which the scattering cross section decreases as $\lambda^{-4}$. Thus we might expect $S$ to decline by more than three orders of magnitude between 400 and 2500 nm. On a log-log plot (not shown), the slope of the scattering curve is increasingly negative at longer wavelengths, reaching about -3 at 2500 nm, so that the Rayleigh limit is not quite reached. The "background" or minimum absorption coefficient here of 0.5 $mm^{-1}$, multiplied by film thickness, is about 0.015. Since, as mentioned earlier, absorptance measurement uncertainties are on the order of 0.01, no definite conclusion can be reached about the actual minimum absorptance. In fact, the underprediction of reflectance over white from 600 to 1400 nm suggests that the film absorptance may be slightly overestimated.

The absorption and backscattering curves are interrupted at four wavelengths in the UV where the 29-$\mu$m thick film is opaque.

Chart I shows a small upward shift in reflectance near 860 nm, where the spectrometer switches from its UV-VIS sensor to its NIR sensor. This indicates that the algorithm to remove such discontinuities (cf. §3.2) is imperfect. The small peaks in absorptance (Chart I) and absorption coefficient (Chart II) at 1700 nm are a feature of the binder, since they appear in many differently pigmented films, including some without substrates. Most polymers have significant IR absorption due to hydrogen vibrations of C-H structures in the 2,000 - 2,400 nm range [45]. Weaker overtones appear in the 1,600 - 1,800 nm regions. Thus, some of the NIR absorptance features seen here are due to the polymer binder. However, it is not unusual for $TiO_2$ pigments to be coated with metal hydroxides, and hydrogen vibrations in $H_2O$ and OH groups may sometimes appear as well.

Chart III indicates that the computed scattering is strong enough to fully diffuse light exiting the bottom of the film ($q_0^i = 1$) at wavelengths $< 1200$ nm, and to fully diffuse the light exiting the top of the film ($q_\delta^j = 1$) at all wavelengths (cf. §2.6). The non-spectral FSR $\sigma = 0.69$ is in

agreement with the theoretical prediction of about 0.65 obtained by assuming a particle diameter of 200 nm, a relative refractive index of $(2.75 + 0i)/1.5$, a PVC of 5%, and a free-space wavelength of 550 nm [46, Fig. 1].

The computed ROB closely matches the measured ROB, but the calculated ROW is about 0.04 low over the range 600 to 1300 nm (Chart IV). We consider three possible explanations.

1. **Inaccurate K-M coefficients.** Underprediction of film reflectance suggests that the algorithm may have overestimated $K$ and/or underestimated $S$. At 1000 nm, $K \approx 0.5$ mm$^{-1}$, $S \approx 200$ mm$^{-1}$, the CRI reflectance of the opaque white background is 0.98, and the observed reflectances over black and white are underpredicted by 0.01 and 0.04, respectively. Eq. (11) indicates that reducing $K$ to zero while leaving $S$ unchanged would increase the over-black and over-white reflectances by 0.007 and 0.02, respectively. Alternately, increasing $S$ fivefold to 1000 mm$^{-1}$ while leaving $K$ unchanged would yield corresponding increases of 0.15 and 0.02. Setting $K$ to zero—which assumes that neither the pigment nor the binder absorb any light whatsoever—would match the over-black reflectances, but leave the ROW underpredicted by 0.02. Setting $S = 1000$ mm$^{-1}$ would yield the same underprediction of ROW, while wildly overpredicting ROB. Of these, the mostly likely explanation is that we have overpredicted $K$.

2. **Inaccurate film-air interface reflectance.** We may have misestimated the film-air interface reflectance used in the Saunderson correction [Eq. (26)] to the predicted reflectances over black and white. We use the theoretical value $\omega_{\text{film}\to\text{air}} = 0.6$ because light exiting the top of a diffusely undercoated film should be fully diffuse. However, since reflectances as low as 0.3 have been observed for diffuse light passing from $n = 1.5$ to $n = 1$ ([43]), we consider the effects of changing $\omega$. The CRI ROB and ROW at 1000 nm are 0.84 and 0.95, respectively. When $\omega = 0.60$, the corresponding observed film reflectances are 0.69 and 0.91. Reducing $\omega$ to 0.5 increases the observed reflectances by 0.05 and 0.01, respectively; increasing $\omega$ to 0.7 decreases them by 0.06 and 0.03. Hence decreasing $\omega$ would aggravate the ROB error much more than it would reduce the ROW error, and increasing $\omega$ would increase both ROB and ROW errors.

3. **Inaccurate background reflectance.** The reflectance of the sample's opaque white back-

ground might be higher than assumed. This is unlikely because the layer of opaque white paint whose reflectance is charted in Fig. 2 is about 1.5-mm thick, and has a spectral transmittance less than 0.01 over virtually the entire solar spectrum. Thus, while making the white undercoating too thin could reduce the reflectance of the sample over white, making the white undercoating too thick should not measurably increase the over-white reflectance.

**B. Carbon Black.** Carbon black (Fig. 3b) is a strongly absorbing pigment with an exponentially-decreasing absorption coefficient that falls half a decade over the solar spectrum (Chart II). It has weak scattering in the UV and visible typical of soot [47], and is essentially non-scattering in the NIR. We note that its measured reflectance over black is approximately 0.04 in the visible and NIR spectra (Chart IV), which is the result expected for a collimated beam passing from air ($n = 1$) to a non-scattering paint ($n = 1.5$). In these spectra, the CRI ROB $R_{f,0}$ computed from Eq. (39) is slightly negative (mean value -0.003); hence, the film is assumed to be nonscattering, the top and bottom diffuse fractions are set to zero (Chart III), and the absorption coefficient is computed in the nonscattering limit from Eq. (25).

The 21-$\mu$m thick film prepared from a diluted carbon black artist paint is quite transparent (Chart I), making it easy to compute $K$ from its transmittance. The forward scattering ratio $\sigma = 0.99$ is largely meaningless because $S = q = 0$ in the NIR. The near-perfect matches between calculated and measured reflectances over black and white match (Chart IV) likely arise from the film's strong absorption, possibly because absorptive attenuation reduces the influence of scattering on film reflectance.

**C. Iron Oxide Red.** Iron oxide red (Fig. 3c) has very strong absorption at wavelengths below 600 nm, and strong scattering at wavelengths longer than 660 nm (Chart II), leading to its dark red appearance over either a white or black background (Chart IV). At wavelengths below 600 nm, the bottom diffuse fraction is forced to zero because the high absorptance ($K > 200$ mm$^{-1}$) generates small values of $i_c(0)$ and $i(c)$, which in turn yield an unphysical (i.e., negative) estimate of diffuse fraction. The matches between predicted and measured reflectances (Chart IV) are quite good, probably because the absorption is never small ($K > 20$ mm$^{-1}$). Other iron oxide red pigments showed less NIR absorption than this pigment (Levinson et al. 2004, Solar Spectral Optical Properties of Pigments, Part II: Survey of Common Colorants).

**D, E. Phthalocyanine Blue and Green.** Phthalocyanine blue (Fig. 3d) and phthalocyanine green (Fig. 3e) are weakly scattering, dyelike pigments with strong absorption in parts of the visible and NIR. Their strong absorptances in the reddish potions of the visible spectrum (Chart I) give each a dark blue or green appearance over a white background, and almost black appearances over a black background (Chart IV). Both of these PVDF-based free films are about 25-$\mu$m thick, have a PVC of about 5%, are fitted with $\sigma \approx 0.8$, and show excellent agreement between measured and calculated reflectances over black. However, the error in ROW is much larger for the green than it is for the blue. At 1280 nm (peak green ROW error), the measured reflectances of green over white and blue over white are each 0.81, but the green film's $K$ and $S$ are each three times larger than those of the blue film. Thus, while the model closely estimates the reflectance of blue over white (error 0.01), its underpredicts the reflectance of green over white by 0.20.

**F. Mica Flakes Coated With Titanium Dioxide.** This pearlescent white film (Fig. 3f) containing mica flakes coated with titanium dioxide is strongly scattering and weakly absorbing in the visible and NIR spectra. Its absorption and backscattering curves are shaped like those of titanium dioxide (Fig. 3a), but $K$ and $S$ are about half an order of magnitude higher and lower, respectively (Chart II). The K-M model is not expected to accurately describe pearlescent films. Since these platelike pigment particles tend to align with the plane of the films, the collimated light that they scatter is unlikely to be uniformly diffuse. This particular pearlescent exhibits one of the poorest fits to ROW, second only to that of the aforementioned phthalo green. The very low $\sigma = 0.1$ may result from specular reflection by the flakes.

## 4.2 Accuracy of K-M Model Vs. Backscattering and Absorption Thicknesses

Fig. 4 charts errors in predicted ROW and ROB vs. backscattering thickness $S\delta$ and absorption thickness $K\delta$ using about 38,000 measurements (87 pigments × 441 wavelengths/pigment). On average (as indicated by the mean error curves in charts [a] and [b]), the model underpredicts both ROW and ROB. As suggested by a prior theoretical error analysis of the K-M model [29], prediction errors are greatest when the film is weakly scattering and/or weakly absorbing. Typical errors ranges (that is, the 95% prediction interval limits) are -0.07 to +0.06 (ROW) and -0.02 to +0.02 (ROB) for weakly scattering films; -0.08 to +0.06 (ROW) and -0.02 to +0.02 (ROB) for weakly absorbing films; -0.04 to +0.01 (ROW) and -0.01 to +0.01 (ROB) for strongly scattering

films; and less than ±0.01 (ROW and ROB) for strongly absorbing films.

### 4.3 Fitted Forward Scattering Ratio

The distribution of forward scattering ratios computed for the 87 coatings shown in Fig. 5 indicates that most of the tested paints are strongly forward scattering ($0.7 \leq \sigma \leq 0.9$).

## 5 Conclusions

We have presented a variant of the two-flux K-M model that determines backscattering and absorption coefficients primarily from the reflectance and transmittance of a film over a void background, using the reflectance over black to obtain an estimate of the forward scattering ratio. Detailed spectral analyses of six representative pigments combined with statistical analyses of about 38,000 spectral measurements indicate several strengths and weaknesses of the model.

1. The K-M coefficients appear qualitatively correct, in the sense that the absorption coefficient reproduces the spectral features of the film's absorptance, and the backscattering coefficient exhibits those of the film's reflectance over black.

2. The film reflectances over white and black backgrounds computed from K-M coefficients closely match corresponding measured values for the first four representative pigments—titanium dioxide white, carbon black, iron oxide red, and phthalo blue—with RMS errors in ROW and ROW not exceeding 0.03 and 0.01, respectively. The last two representative pigments—phthalo green and pearlescent bright white—exhibit large errors (RMS 0.10) in predicted ROW.

3. The model on average underpredicts both ROB and ROW, with errors on the order of about ±0.07 for ROW and ±0.02 for ROB when a film is weakly scattering and/or weakly absorbing. The latter feature suggests that the model is likely to underestimate the NIR reflectance of cool (weakly NIR absorbing) films.

## Acknowledgements

This work was supported by the California Energy Commission (CEC) through its Public Interest Energy Research Program (PIER), by the Laboratory Directed Research and Development (LDRD) program at Lawrence Berkeley National Laboratory (LBNL), and by the Assistant Secretary for Renewable Energy under Contract No. DE-AC03-76SF00098. The authors wish to thank CEC Commissioner Arthur Rosenfeld and PIER program project managers Nancy Jenkins and Chris Scruton for their support and advice. Special thanks go also to Mark Levine, director of the Environmental Energy Technologies Division at LBNL, and Stephen Wiel, head of the Energy Analysis Department at LBNL, for their encouragement and support in the initiation of this project. We also wish to thank the following people for their assistance: Kevin Stone and Melvin Pomerantz, LBNL; Michelle Vondran, John Buchko, and Robert Scichili, BASF Corporation; Richard Abrams, Robert Blonski, Ivan Joyce, Ken Loye, and Ray Wing, Ferro Corporation; Tom Steger and Jeffrey Nixon, Shepherd Color Company; and Robert Anderson, Liquitex Artist Materials.

## References

[1] R.F. Brady and L.V. Wake. Principles and formulations for organic coatings with tailored infrared properties. *Progress In Organic Coatings*, 20(1):1–25, 1992.

[2] Gil Burkhart, Terry Detrie, and Dan Swiler. When black is white. *Paint and Coatings Industry Magazine*, January 2001.

[3] Terrence R. Sliwinski, Richard A. Pipoly, and Robert P. Blonski. Infrared reflective color pigment. U.S. Patent 6,174,360 B1, Jan 16 2001.

[4] Jeffrey D. Nixon. The chemistry behind 'Cool Roofs'. *eco-structure*, 1(1):63–65, 2003.

[5] Ferro Corporation. Cool Colors$^{TM}$ and Eclipse$^{TM}$ pigments. *http://ferro.com.*

[6] Shepherd Color Company. Arctic infrared-reflecting pigments. *http://shepherdcolor.com.*

[7] BASF Industrial Coatings. Ultra-Cool$^{TM}$: the new heat reflective coatings from BASF. *http://www.ultra-cool.basf.com.*

[8] Custom-Bilt Metals. Ultra-Cool$^{TM}$ coating saves energy and money on Custom-Bilt Metals roofing systems. *http://www.custombiltmetals.com*.

[9] MCA Tile. MCA Tile ENERGY STAR roof products. *http://www.mcatile.com*.

[10] ASTM. ASTM G 173-03: standard tables for reference solar spectral irradiance at air mass 1.5: direct normal and hemispherical on 37° tilted surface. Technical report, American Society for Testing and Materials, 2003.

[11] R. Levinson, H. Akbari, S. Konopacki, and S. Bretz. Inclusion of cool roofs in nonresidential Title 24 prescriptive requirements. Report LBNL-50451, Lawrence Berkeley National Laboratory, Berkeley, CA, 2002.

[12] R. Levinson, H. Akbari, S. Konopacki, and S. Bretz. Inclusion of cool roofs in nonresidential Title 24 prescriptive requirements. *Journal of Energy Policy*, in press, 2003.

[13] Paul Berdahl, Hashem Akbari, and Leanna S. Rose. Aging of reflective roofs: soot deposition. *Applied Optics*, 41(12):2355–2360, 2002.

[14] S. Konopacki, H. Akbari, M. Pomerantz, S. Gabersek, and L. Gartland. Cooling energy savings potential of light-colored roofs for residential and commercial buildings in 11 US metropolitan areas. Report LBNL-39433, Lawrence Berkeley National Laboratory, Berkeley, CA, 1997.

[15] Yasuhiro Genjima and Haruhiko Mochizuki. Infrared radiation reflector and infrared radiation transmitting composition. U.S. Patent 6,366,397 B1, Apr 16 2002.

[16] Max Born and Emil Wolf. *Principles of Optics*. Cambridge University Press, 7th edition, 1999.

[17] H.C van de Hulst. *Light Scattering by Small Particles*. Dover Publications, 1981.

[18] Craig F. Bohren and Donald R. Huffman. *Absorption and Scattering of Light by Small Particles*. Wiley.

[19] L.E. McNeil and R.H. French. Multiple scattering from rutile $TiO_2$ particles. *Acta Materialia*, 48:4571–4576, 2001.

[20] A. Schuster. Radiation through a foggy atmosphere. *Astrophys. J.*, 21(1), 1905.

[21] P. Kubelka. New contributions to the optics of intensely light-scattering materials, part I. *Journal of the Optical Society of America*, 38:448, 1948.

[22] Gustav Kortum. *Reflectance Spectroscopy: Principles, Methods, Applications*. Springer, 1969.

[23] Craig F. Bohren. Multiple scattering of light and some of its observable consequences. *American Journal of Physics*, 55(6):524–533, June 1987.

[24] Deane B. Judd. *Color in Business, Science, and Industry*. John Wiley and Sons, 1952.

[25] Ruth M. Johnston. *Pigment Handbook*, volume III, chapter D-b ("Color Theory"), pages 229–288. John Wiley and Sons, 1988.

[26] J.W. Ryde. The scattering of light by turbid media: Part I. *Proceedings of the Royal Society of London: Series A*, 131(817):451–464, May 1931.

[27] B. Maheu, J.N. Letoulouzan, and G. Gouesbet. Four-flux models to solve the scattering transfer equation in terms of Lorenz-Mie parameters. *Applied Optics*, 23(19):3353–3362, October 1984.

[28] William E. Vargas. Generalized four-flux radiative transfer model. *Applied Optics*, 37(13):2615–2623, 1998.

[29] William E. Vargas and Gunnar A. Niklasson. Applicability conditions of the Kubelka-Munk theory. *Applied Optics*, 36(22):5580–5586, August 1997.

[30] Y.S. Touloukian, D.P. DeWitt, and R.S. Hernicz. *Thermal Radiative Properties: Coatings*, volume 9 of *Thermophysical Properties of Matter*. IFI/Plenum, 1972.

[31] Peter A. Lewis. *Pigment Handbook*, volume I. John Wiley and Sons, 1988.

[32] Ralph Mayer. *The Artist's Handbook of Materials and Techniques*. Viking Penguin, 5th edition, 1991.

[33] Roy S. Berns. *Billmeyer and Saltzman's Principles of Color Technology*. John Wiley and Sons, 3 edition, 2000.

[34] William E. Vargas and Gunnar A. Niklasson. Generalized method for evaluating scattering parameters used in radiative transfer models. *Journal of the Optical Society of America: A*, 14(9):2243–2252, September 1997.

[35] L.E. McNeil and R.H. French. Light scattering from red pigment particles: multiple scattering in a strongly absorbing system. *Journal of Applied Physics*, 89(1):283–293, 2001.

[36] Avantes. Mix2Match color matching software. *http://avantes.com*.

[37] Color-Tec. Color formulation software. *http://color-tec.com*.

[38] Datacolor. Paintmaker laboratory software. *http://datacolor.com*.

[39] GretagMacbeth. Propalette plastics/coatings color formulation and quality control software. *http://gretagmacbeth.com*.

[40] Eugene Allen. *Optical Radiation Measurments*, volume 2, chapter 7 ("Colorant Formulation and Shading"), pages 289–336. Academic Press, 1980.

[41] J.L. Saunderson. Calculation of the color of pigmented plastics. *Journal of the Optical Society of America*, 34(167):727–736, 1942.

[42] J.W. Ryde and B.S. Cooper. The scattering of light by turbid media: Part II. *Proceedings of the Royal Society of London. Series A*, 131(817):464–475, May 1931.

[43] D. Spitzer and J.J. Ten Bosch. A simple method for determination of the reflection coefficient at the internal surfaces of turbid slabs. *Optics Communications*, 9(3):311–314, November 1973.

[44] Ame Roos, Carl G. Ribbing, and Mikael Bergkvist. Anomalies in integrating sphere measurements on structured samples. *Applied Optics*, 27(18):3828–3832, September 1988.

[45] R.T. Conley. *Infrared Spectroscopy*. Allyn and Bacon, Inc., Boston, 2nd edition, 1972.

[46] William E. Vargas and Gunnar A. Niklasson. Forward-scattering ratios and average pathlength parameter in radiative transfer models. *J. Phys: Condens. Matter*, 9:9083–9096, 1997.

[47] M. Y. Choi, G. W. Mulholland, A. Hamins, and T. Kashiwagi. Comparisons of the soot volume fraction using gravimetric and light extinction techniques. *Combust. Flame*, 102:161–169, 1995.

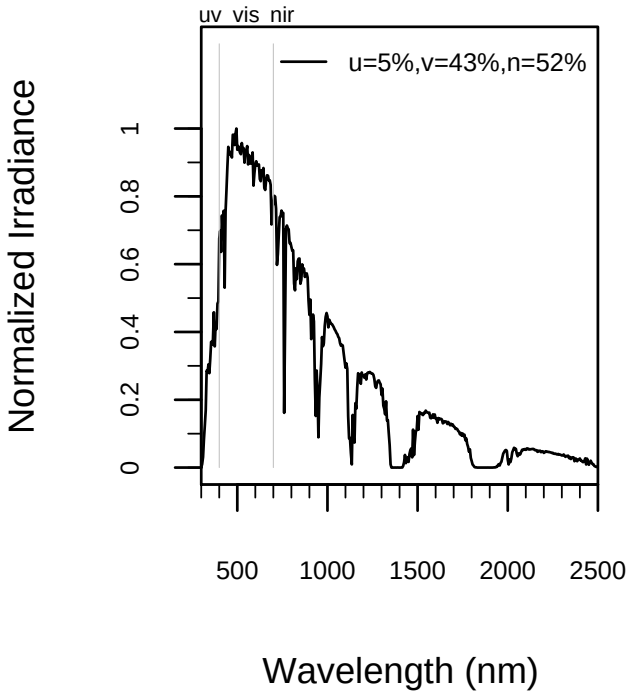


Figure 1: Air mass 1.5 hemispherical solar spectral irradiance typical of North American insolation (5% ultraviolet, 43% visible, 52% near-infrared) [10].

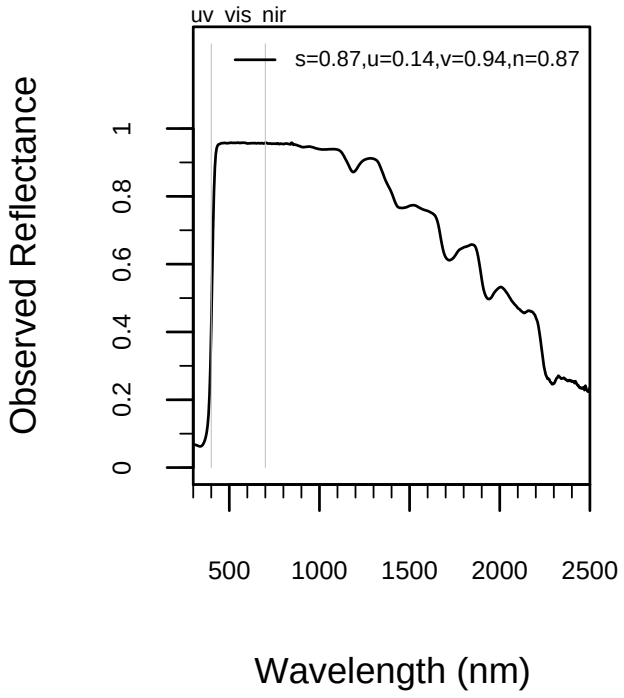


Figure 2: Observed spectral reflectance of an opaque white background (1.5-mm thick $TiO_2$-white acrylic paint film).

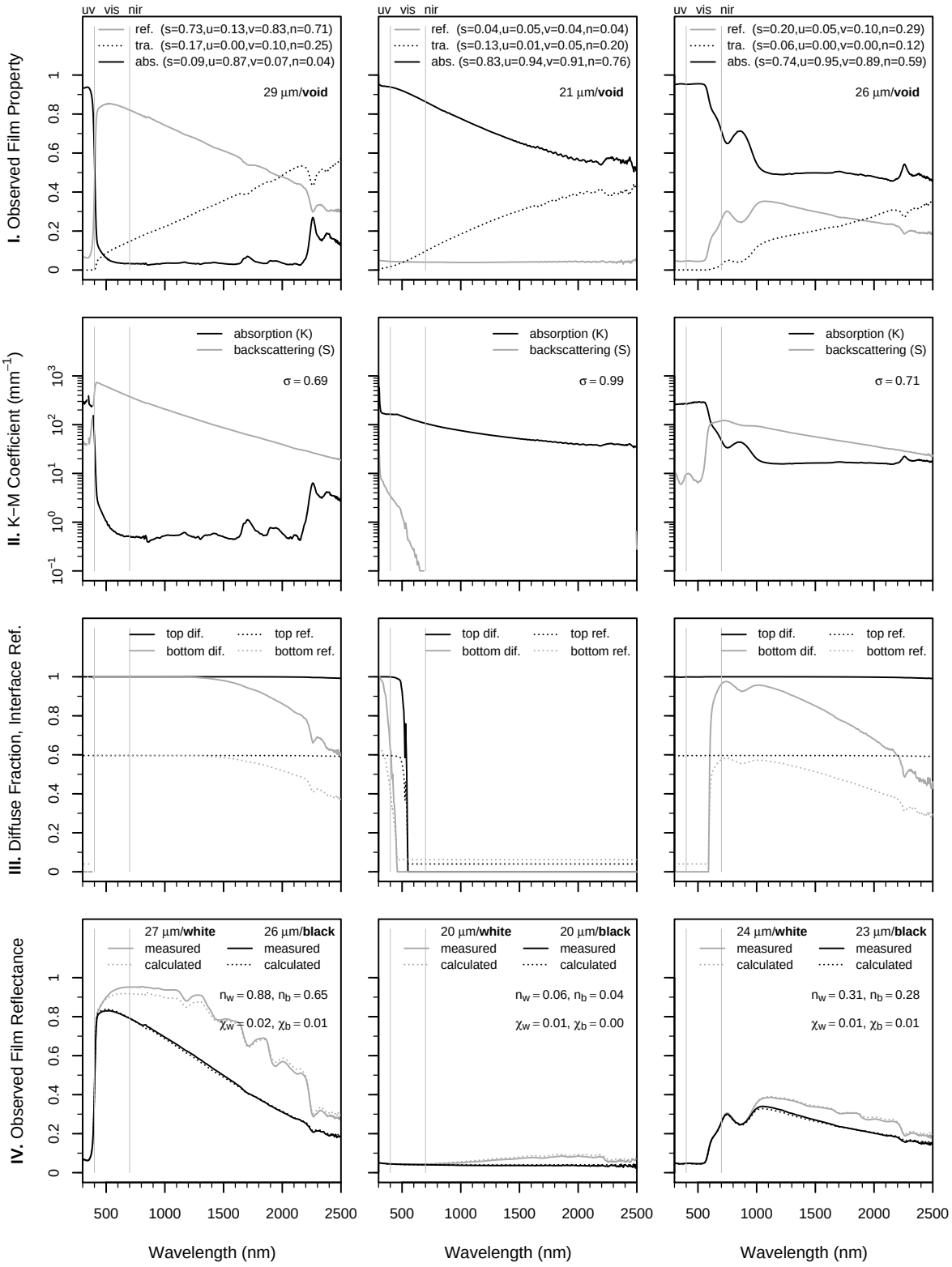


Figure 3: (i/ii) Measurements and model calculations for six coatings: (a) titanium dioxide white, (b) carbon black, (c) iron oxide red, (d) phthalo blue, (e) phthalo green, and (f) pearlescent white. Shown from top to bottom are (I) measured reflectance, transmittance, and absorptance of film with void background; (II) Kubelka-Munk backscattering and absorption coefficients $S$ and $K$, and non-spectral forward scattering ratio $\sigma$; (III) computed diffuse fraction and interface reflectance of fluxes exiting top and bottom of film; and (IV) measured and computed film reflectances over white [w] and black [b] backgrounds, measured NIR reflectance $N$, and the RMS error $\chi$.

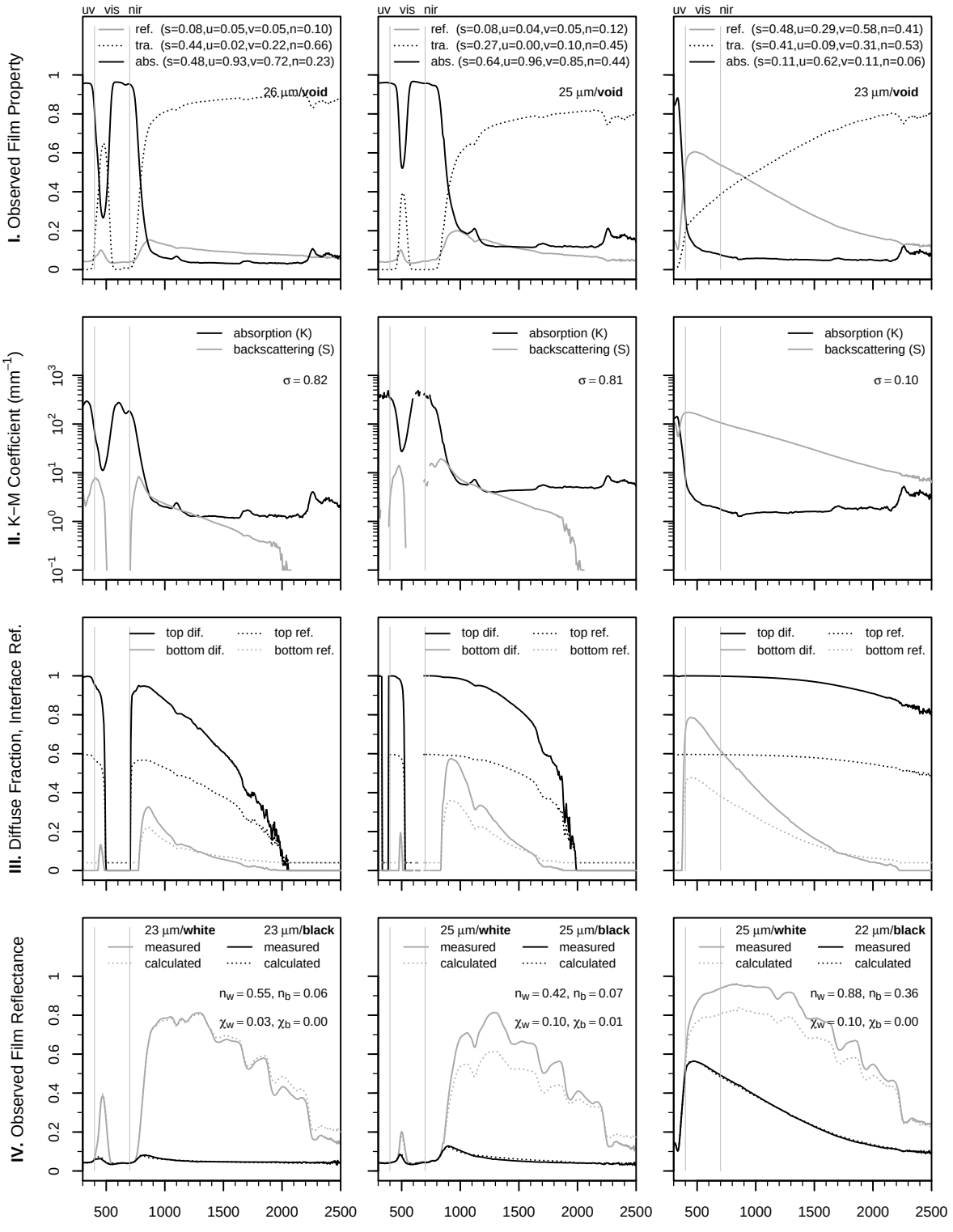


**(d)**
**Phthalo Blue (ii)**
**Toyo Lionel BF−28201 (PB 15)**
**5% PVC**
**{phthalocyanine blue}**

**(e)**
**Phthalo Green (ii)**
**Clariant GT−674−D Endurophthal Green B (PG 7)**
**4% PVC**
**{phthalocyanine green}**

**(f)**
**Bright White (Pearlescent)**
**Engelhard Exterior Mearlin 139X Bright White**
**11% PVC**
**{mica + titanium dioxide}**

Figure 3: (ii/ii) continued.

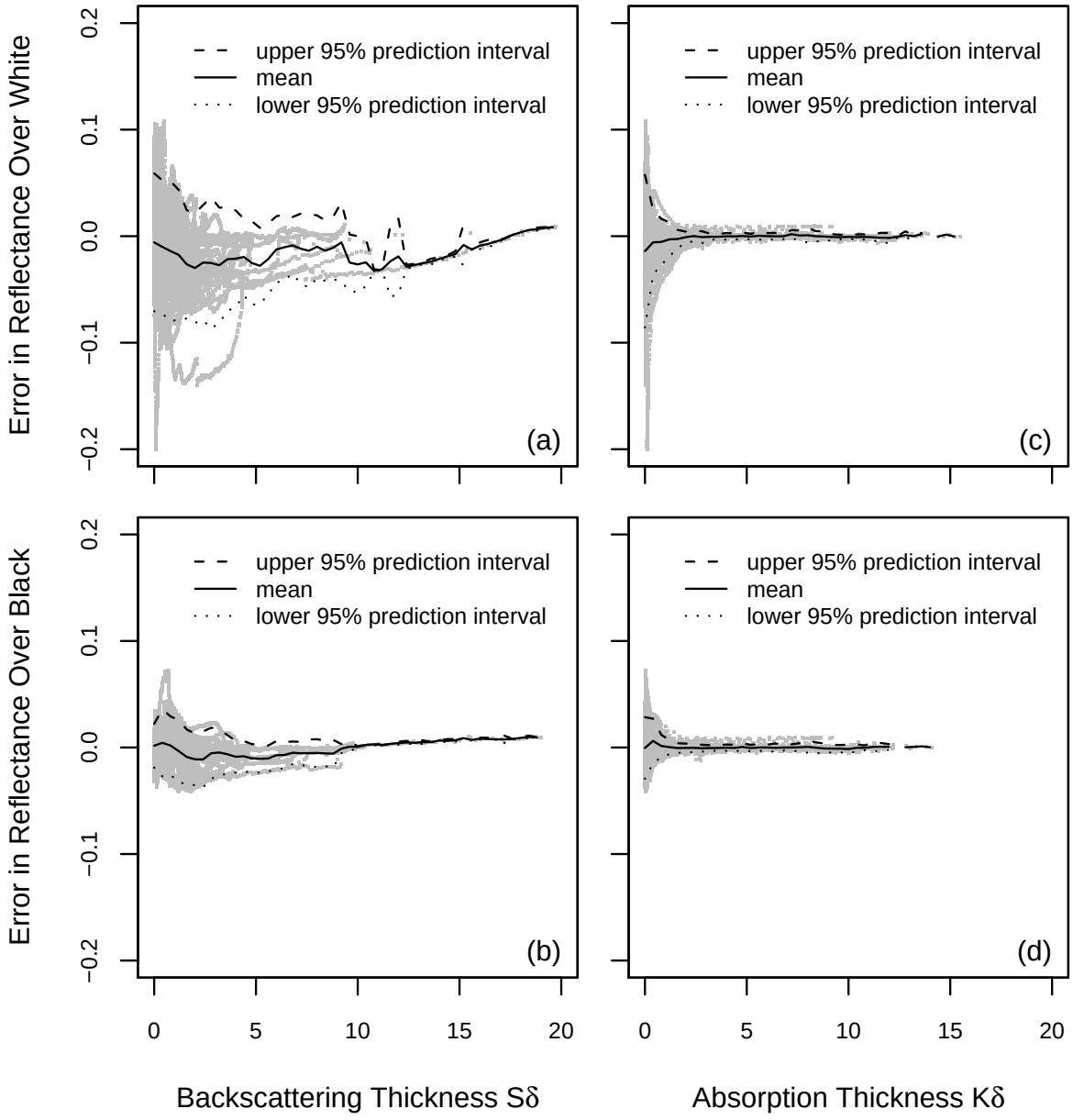


Figure 4: Errors in reflectances computed from Kubelka-Munk coefficients. Shown are (a, b) computed - measured values of observed film reflectance over (white, black) backgrounds vs. backscattering thickness $S\delta$; and (c, d) the same errors vs. absorption thickness $K\delta$.

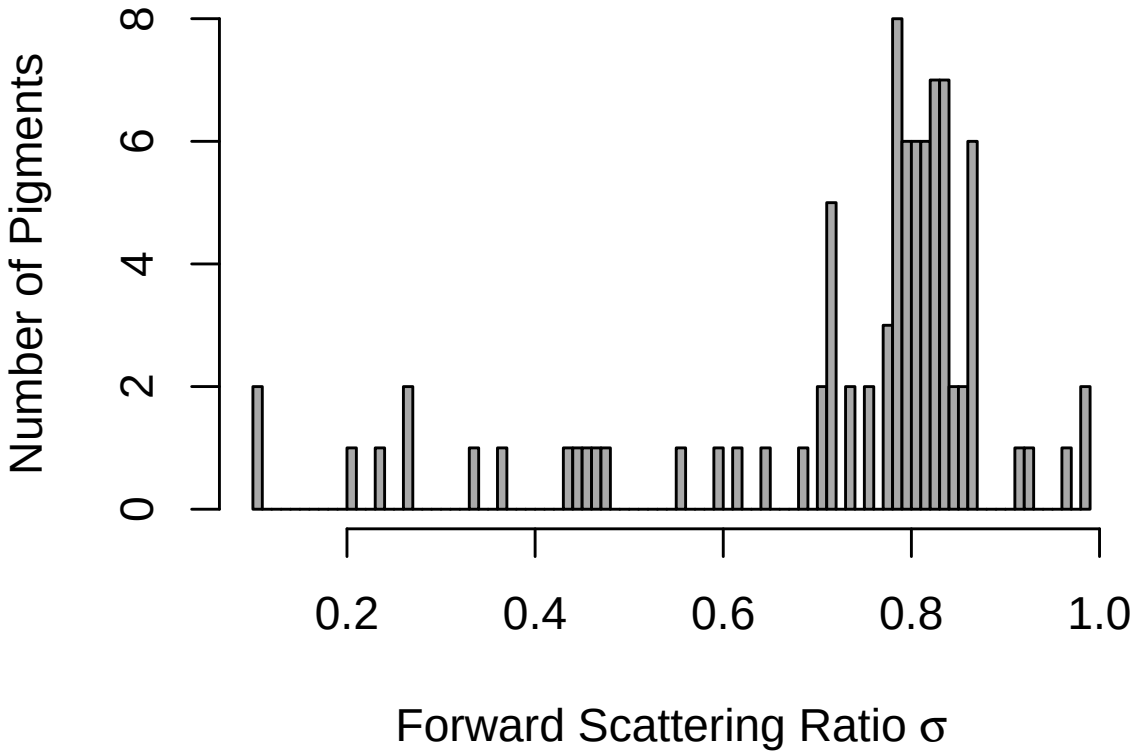


Figure 5: Frequency distribution of non-spectral forward scattering ratio $\sigma$. Most pigments characterized were strongly forward scattering.